Emittance preservation in the presence of ion motion for low-to-high energy stages of a plasma based accelerator

Yujian Zhao, 1,2 Lance Hildebrand, 1,2 Weiming An, 3 Xinlu Xu, 5,6 Fei Li, 4
Thamine N. Dalichaouch, 1,2 Qianqian Su, 2 Chan Joshi, 2 and Warren B. Mori, 1,2

1 Department of Physics and Astronomy, University of California Los Angeles,
Los Angeles, California 90095, USA

2 Department of Electrical and Computer Engineering, University of California Los Angeles,
Los Angeles, California 90095, USA

3 Department of Astronomy, Beijing Normal University, Beijing 100875, China
4 Department of Engineering Physics, Tsinghua University, Beijing 100084, China
5 State Key Laboratory of Nuclear Physics and Technology, and Key Laboratory of HEDP of the Ministry
of Education, CAPT, Peking University, Beijing, 100871, China
6 Beijing Laser Acceleration Innovation Center, Beijing 100871, China

(Received 8 April 2023; accepted 20 November 2023; published 14 December 2023)

Plasma based acceleration (PBA) is being considered for a next generation linear collider (LC). In typical PBA-LC designs, the extreme beam parameters are expected to trigger background ion motion, which can lead to longitudinally varying nonlinear focusing forces and result in emittance growth of the beam. While various schemes have been proposed to mitigate this at low beam energies, a solution to minimize the emittance growth in the later high energy stages of a multistage electron acceleration arm is yet to be found. In this paper, we propose to use an adiabatic plasma density ramp as a matching section that is able to match the witness electron beam to the low-density plasma entrance, where the beam initially has a large matched spot size so the ion motion effects are relatively small. As the beam propagates in the plasma density upramp (downramp), it is adiabatically focused (defocused) and its distribution maintains an equilibrium distribution throughout the entire process even when severe ion collapse has occurred. Simulation results from QPAD show that within a single acceleration stage, this concept can limit the projected emittance growth to only $\sim 2\%$ for a 25 GeV, 100 nm normalized emittance witness beam and $\sim 20\%$ for a 100 GeV, 100 nm normalized emittance witness beam.

DOI: 10.1103/PhysRevAccelBeams.26.121301

Research on plasma based acceleration (PBA) has made great progress during the past few decades [1]. In PBA, an intense particle or laser beam is used to form a plasma wake that accelerates a second electron beam that is properly loaded inside the wake. In the blowout regime of PBA [2,3], the wakefield provides an ideal focusing force on an electron beam that is linear in transverse position r and independent of the longitudinal position $\xi = ct - z$, while the accelerating field is independent of r. For such conditions, an accelerating electron beam can be matched to the focusing force thereby almost perfectly preserving the beam's slice and projected normalized emittance ϵ_n [4]. The evolution of the beam's rms spot size, σ , in a linear focusing force of the ion column, is described by $\frac{\partial^2 \sigma}{\partial z^2} = \frac{\epsilon_n^2}{\gamma^2 \sigma^3} (1 - \frac{\gamma^2 k_\beta^2}{\epsilon_n^2} \sigma^4)$, where $\epsilon_n = \gamma \epsilon$ is the normalized

Published by the American Physical Society under the terms of the Creative Commons Attribution 4.0 International license. Further distribution of this work must maintain attribution to the author(s) and the published article's title, journal citation, and DOI. emittance (hereafter referred to as the emittance), γ is the relativistic Lorentz factor, $k_{\beta}=\frac{\omega_p}{\sqrt{2\gamma}c}$ is the betatron wave number, and ω_p is the plasma frequency. The matched spot size is then given by $\frac{\gamma^2 k_{\beta}^2}{c_n^2} \sigma_m^4 = 1$ [5] leading to

$$\sigma_m = (2/\gamma)^{1/4} (\epsilon_n c/\omega_p)^{1/2}. \tag{1}$$

The beam's σ_m in the plasma is much smaller than conventional focusing optics can provide. This mismatch leads to large emittance growth when there is energy spread.

To overcome this, it has been proposed to use a tailored short plasma ramp or an adiabatic plasma ramp [6–12] to transition the beam from a large spot size to a small matched spot size in the acceleration stage.

In order to build a TeV-class linear collider (LC), the luminosity, $L = fN^2/4\pi\sigma_x\sigma_y$, must be as large as $\sim 10^{34}$ cm⁻² s⁻¹, where *N* is the number of particles in each colliding bunch, *f* is the repetition rate of collisions, and $\sigma_{x,y}$ is the spot size of the bunch at the interaction point. To achieve such a luminosity, a beam with ~ 1 nC charge

and ~100 nm emittance has been proposed [13]. For such a beam, the transverse Coulomb field of a matched spot size can pull the ions inward during the transit time of the beam [14,15]. This results in a ξ (slice) dependent, transversely nonlinear focusing force, which can result in emittance growth. The degree of ion motion is quantified through the amount of phase advance of an ion from the beam's field [14,15], $\Phi = \sqrt{4\pi e^2 Z n_b/M} (\sigma_z/c) \equiv \omega_{bi} (\sigma_z/c)$, where n_b is the peak beam density, Z is the ionization state of the ion, M is the ion mass, and σ_z is the rms bunch length. Simulations have shown that matching the beam directly to a uniform plasma causes ~80% projected emittance growth for typical LC parameters [16].

Several ideas have been proposed and studied to mitigate the emittance growth even further in the presence of ion motion. Reference [17] proposed to use a plasma matching section with an adiabatically decreasing ion mass. Reference [18] proposed slice-by-slice matching the transverse beam phase space distribution to the nonlinear ion motion-perturbed plasma wakefields. However, these ideas may be difficult to realize experimentally. Reference [19] proposed an adiabatic matching procedure where the beam is injected with a low enough energy that ion motion effects are initially small. However, this idea will only work at the initial stage.

In this paper, we present a scheme that is able to achieve emittance preservation in the presence of ion motion that is applicable to high-energy, high-density electron bunches required in a multistage PBA. We use adiabatic plasma density upramps and downramps to match the witness beam into and out of a uniform density (plateau). We show that this method can preserve the witness beam emittance from start to end, even though there is a significant amount of slice dependent ion motion triggered in the plateau. By properly choosing the beam's Courant-Snyder (CS) parameters at the plasma entrance, the emittance growth can be mitigated even for more general density ramps that are not adiabatic at lower densities.

Within an ion channel, the matched CS parameters $\alpha_m(z)$ and $\beta_m(z)$ are [9,12,20]

$$\beta_m(z) = \sqrt{2\gamma}c/\omega_p(z), \qquad \alpha_m(z) = -\frac{1}{2}\beta'_m(z).$$
 (2)

An adiabaticity parameter can be defined as $\mathcal{A} = |\alpha_m|$ [9,20], which describes how adiabatic the plasma density is changing from the beam's point of view. The adiabatic condition is given by $\mathcal{A} < 1$.

In a density upramp (downramp), α_m is positive (negative). Therefore, we design an adiabatic plasma density upramp with α_m linearly decreasing to 0 (at the plateau) so that the transition from the upramp to the plateau is smooth. Based on this assumed linear dependence of α_m , we can integrate the CS equations to solve for the density dependence of the upramp

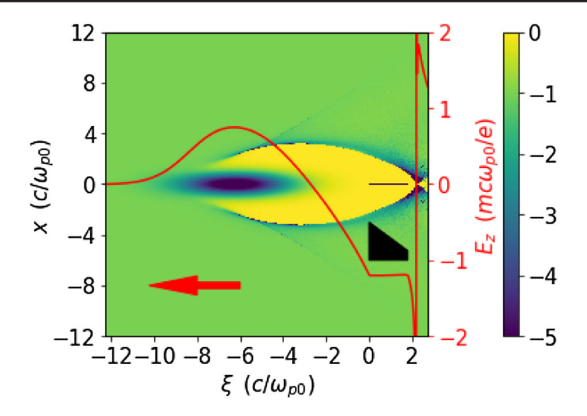


FIG. 1. A snapshot of the wake and beams in the density plateau. The color bar corresponds to the charge density for the plasma electrons, drive beam, and witness beam. The witness beam has a trapezoidal longitudinal current profile (black) in order to flatten the accelerating field E_z (on-axis lineout in red).

$$\frac{n(z)}{n_0} = \left(1 + \frac{\alpha_{mi}(z - L)^2}{\beta_{m0}L}\right)^{-2},\tag{3}$$

where β_{m0} is β_m evaluated within the density plateau, and the adiabaticity parameter at the entrance, α_{mi} , depends on the choice of the plasma density at the entrance by Eq. (3).

We demonstrate this scheme through fully nonlinear, self-consistent simulations of a single plasma wakefield acceleration based linear collider (PWFA-LC) stage using OPAD [21], a quasistatic particle-in-cell (PIC) code based on the QuickPIC framework [22,23] that expands the fields in azimuthal harmonics and truncates the expansion at a desired number. We use very fine resolution in r so that the physics of ion motion can be fully resolved. The (r, ξ) simulation box has dimensions $12k_{p0}^{-1} \times 15k_{p0}^{-1}$ (see Fig. 1), and cell sizes $5 \times 10^{-4} k_{p0}^{-1} \times 10^{-2} k_{p0}^{-1}$, where $k_{p0} = \omega_{p0}/c$ is the plasma wave number. The witness beam consists of 10⁷ numerical particles. The beam particles are pushed every 3D time step $\Delta t = 10\omega_{p0}^{-1}$. Both plasma electrons and ions are initialized at 4 locations uniformly spaced per r, ξ cell with 16 particles distributed in the azimuthal direction. Unless otherwise noted, we only keep the lowest m = 0azimuthal mode thereby assuming axisymmetric beam and plasma distributions.

For the physical parameters, we use a preformed hydrogen plasma with density $n_0 = 10^{17}$ cm⁻³ for the uniform acceleration section. It is 67.3 cm $(4 \times 10^4 \ k_{p0}^{-1})$ long. The drive beam has an initial energy of 25 GeV, 3.0×10^{10} electrons (4.8 nC), an emittance of $\epsilon_n = 1$ mm, and a tri-Gaussian density profile with $\sigma_r = 10.4$ µm and $\sigma_z = 30$ µm. It is thus matched to the uniform acceleration section. The drive beam's peak density $n_{b0} = 5.89n_0$ can produce a fully blown-out wake but not trigger any ion motion. The drive beam is set to be nonevolving (it is represented by a specified current profile) to isolate the physics. The witness beam also has an initial energy of

25 GeV, but an $\epsilon_n=100$ nm, and a trapezoidal longitudinal current profile that flattens the wake [24] ranging from $I_{b,head}=25.26$ kA at the head to $I_{b,tail}=6.42$ kA at the tail. Its length is $1.8k_{p0}^{-1}$ (30.3 µm), so the total charge is 1.0×10^{10} electrons (1.6 nC). The head of the witness beam is located $6.25k_{p0}^{-1}$ (105.2 µm) behind the center of the drive beam where it optimally loads the wake [24,25], as shown in Fig. 1. The nearly constant accelerating field along the witness beam is around $E_z=-1.2mc\omega_{p0}/e$ for all beam slices. The witness beam is initialized with no energy spread to isolate physics.

For the upramp, we choose $\alpha_{mi}=1$ and then choose either L or n_i/n_0 , with the other following from Eq. (3). Here, we place an adiabatic plasma density upramp with $L=50.5~{\rm cm}(3\times 10^4 k_{p0}^{-1})$ before the density plateau and a symmetric downramp after the density plateau. For this L, $n_i/n_0=10^{-4}$. The entire plasma density profile is shown by the black solid curve in Fig. 2(a).

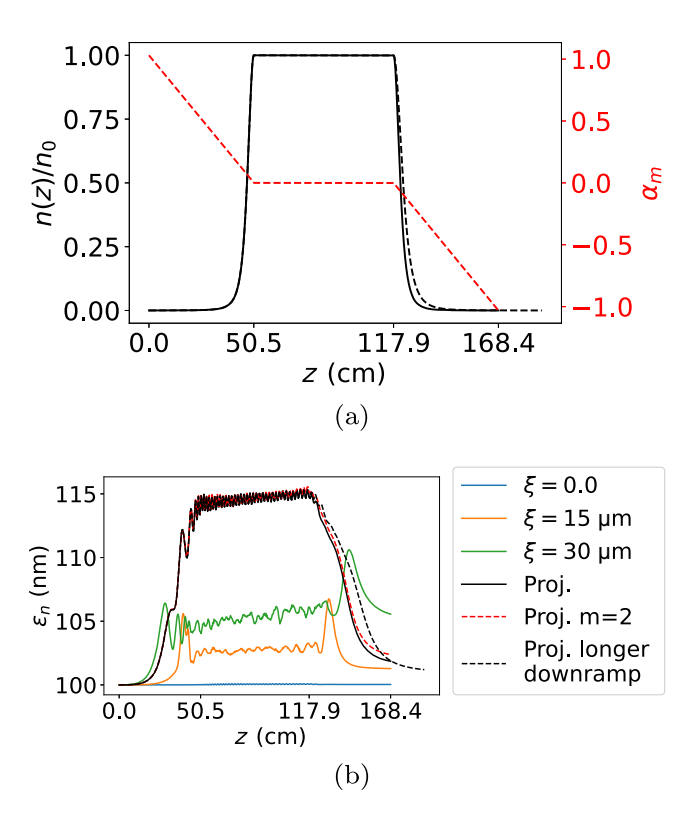


FIG. 2. (a) The resulting adiabatic plasma density profile (solid black) based on a linear ramp for α_m . The black dashed downramp takes into account the energy doubling of the witness beam. (b) Evolution of the projected emittance (solid black) and selected slice emittances. The witness beam's head and tail are located at $\xi=0,30~\mu\mathrm{m}(1.8k_{p0}^{-1})$, respectively. The red dashed curve shows the evolution of the projected emittance when three azimuthal modes, m=0,1,2, are kept in a QPAD simulation. The black dashed curve shows the evolution of the projected emittance for the case where the black dashed downramp in (a) is used.

In Fig. 2(b), we show the evolution of the projected emittance (black solid) and the slice emittance at the head (blue), middle (orange), and tail (green) of the witness beam. The thickness of the slices is chosen to be $\Delta \xi = 0.1 k_{p0}^{-1}$. The projected emittance steadily grows in the density upramp, then grows very slowly in the density plateau [19], but eventually decreases in the density downramp, with only a ~2% net emittance growth at the exit of the plasma downramp.

To understand the evolution of the projected emittance, we need to investigate how the phase space evolves within individual slices. At the entrance of the plasma upramp, the density is low, and according to Eq. (1), σ_m is large. The beam's peak density (and self-electric field) is therefore low. As a result, ion motion is initially small, and the beam is essentially matched to the unperturbed linear focusing force. In Fig. 3, we present the focusing force at the head $(\xi = 0)$, middle $(\xi = 15 \mu m)$, and tail $(\xi = 30 \mu m)$ of the

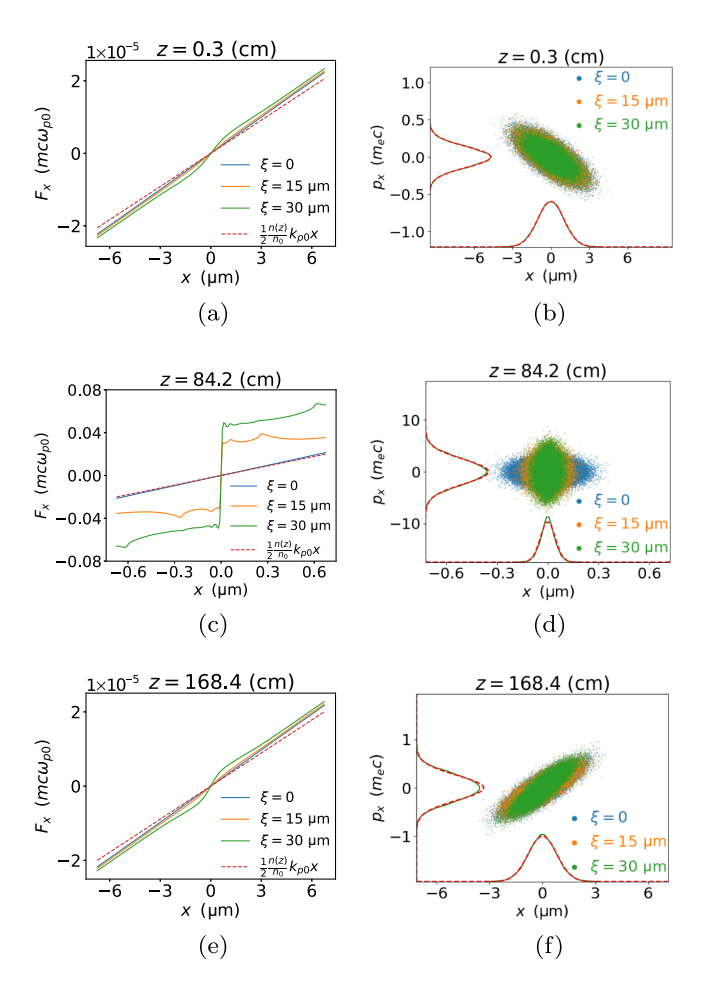


FIG. 3. (a),(c),(e) Focusing force in \hat{x} at different longitudinal ξ positions for different z propagation distances. (b),(d),(f) Phase space ellipses corresponding to different longitudinal slices. The colors of each particle correspond to the colors of the focusing force. The distribution for p_x and x are shown for the $\xi=30~\mu m$ slice (green curve) and a Gaussian fits that match the standard deviation are shown as red dashed lines.

witness beam for three propagation distances that correspond to the entrance of upramp, middle of plateau, and exit of downramp. We also show the phase space for slices centered at the same ξ locations (represented by different colored dots). In the upramp region before there is any ion motion, Fig. 3(a) shows that the focusing force at each slice is nearly the same as from the ion column. In Fig. 3(b), the phase space distributions for each slice all overlap as well.

As the beam propagates into the ramp, the plasma density slowly increases, causing the beam to be adiabatically compressed. This leads to a higher peak density (thus a stronger self-electric field), so ion motion is adiabatically triggered. In this process, the beam's distribution will slowly and continuously evolve to match the local nonlinear focusing force. Each slice of the beam experiences a different transverse focusing force and therefore evolves differently. At the density plateau, we can see that the focusing forces at different ξ are different [Fig. 3(c)], leading to different evolution for each phase space ellipse [Fig. 3(d)].

Due to the nonlinear focusing force, there is some emittance growth within each slice. However, in contrast to the growth due to the phase mixing that occurs for initially unmatched beams, this growth is reversible in the downramp [26]. Due to the nonlinear focusing force, the distributions of the beam particles are no longer Gaussian. We can see the green curves deviate from the red dashed curves in Fig. 3(d). These non-Gaussian profiles lead to larger values for the slice emittance in the density plateau, as shown in Fig. 2(b). In addition, slices at head, middle, and tail of the beam feel different focusing forces, so their corresponding phase space ellipses no longer overlap with each other, resulting in a projected emittance growth that is much larger than for each slice.

In the downramp, the beam's evolution is the reverse of that in the upramp; the beam's spot size slowly expands so the peak density becomes lower, the ion motion retreats, and the focusing force becomes roughly linear and longitudinally independent again [see Fig. 3(e)]. Therefore, the non-Gaussian distributions that led to a slight increase in the emittance of each slice are reversed and the different phase space ellipse evolutions for different longitudinal slices gradually also reverse such that the slices overlap with each other again at the exit [Fig. 3(f)]. After the entire acceleration stage, the witness beam gained 25 GeV while maintaining a very small energy spread $(\sigma_\gamma/\bar{\gamma}\sim 0.1\%$ at the exit), with only a 2% projected emittance growth.

We also ran another simulation that includes the m=0,1,2 modes. The projected emittance is shown in the red dashed curve in Fig. 2(b), which is very similar to the m=0 mode only result (solid black curve). This indicates that there is no hosing growth from noise during the entire stage.

The downramp is symmetric to the upramp for simplicity. However, the witness beam's energy doubled after being accelerated in the plateau, so β_{m0} becomes $\sqrt{\gamma_f/\gamma_i} = \sqrt{2}$ times larger, where γ_i and γ_f denote the witness beam's

energy at the entrance and the exit of the plateau, respectively. From Eq. (3), we can see that in order to keep the same adiabaticity, the length of the downramp should be $\sqrt{2}$ times that of the upramp, shown by the black dashed curve in Fig. 2(a). Using this downramp instead, the evolution of the projected emittance in the downramp is shown in Fig. 2(b). We can see that the projected emittance growth at the exit of the downramp is even smaller.

A fully adiabatic ramp is challenging to construct, therefore, we consider more general ramp profiles. Specifically, we use the following fifth order polynomial:

$$n(z) = n_0 \left[6\left(\frac{z}{L}\right)^5 - 15\left(\frac{z}{L}\right)^4 + 10\left(\frac{z}{L}\right)^3 \right] (0 \le z \le L).$$
 (4)

The length of the ramp is the same as before, L=50.5 cm $(3\times 10^4 k_{p0}^{-1})$. The density upramp is shown as the blue curve in Fig. 4. The density downramp is still chosen to be symmetric to that of the upramp. Unlike the fully adiabatic ramp given by Eq. (3), the density of the ramp vanishes at the entrance. As a result, both the matched spot size defined in Eq. (1), i.e., β_m , and the adiabaticity parameter, α_m , diverge toward infinity as the density approaches 0.

Despite the divergence of the adiabaticity at the beginning of the ramp, we find it is still possible to roughly match the beam. In the absence of ion motion and any longitudinal acceleration, the CS parameters evolve according to [27]:

$$\frac{1}{2}\beta\beta'' - \frac{1}{4}\beta'^2 + \beta^2 k_{\beta}^2 = 1, \qquad \alpha = -\frac{1}{2}\beta'.$$
 (5)

Starting from the matched CS parameters at the density plateau: $\beta_m = \sqrt{2\gamma} k_{p0}^{-1}$, $\alpha_m = 0$ as the initial conditions for β and α , we numerically integrate Eq. (5) backward along the upramp [5] (see dashed curves in Fig. 4), and get β_i , α_i

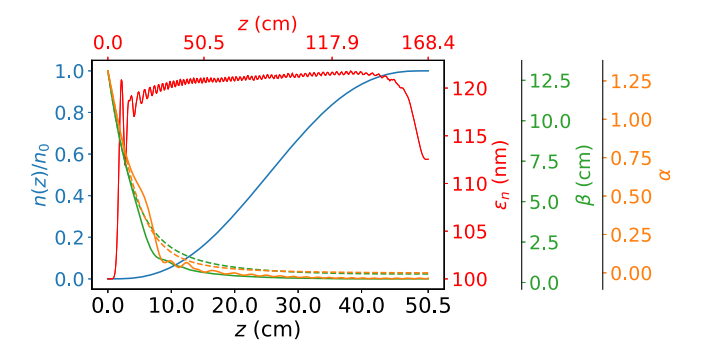
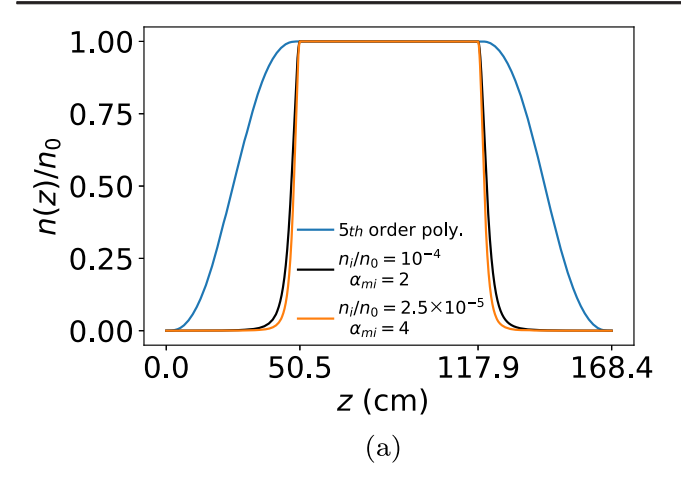


FIG. 4. The density profile for the fifth order polynomial upramp (blue) and the evolution of the CS parameters. The solid green and orange curves are the β and α of the witness beam from the QPAD simulation; and the dashed curves are from numerical backward propagation. The red curve shows the projected emittance evolution in the entire plasma density (upramp, plateau, and downramp) profile shown as the blue curve in Fig. 5(a).



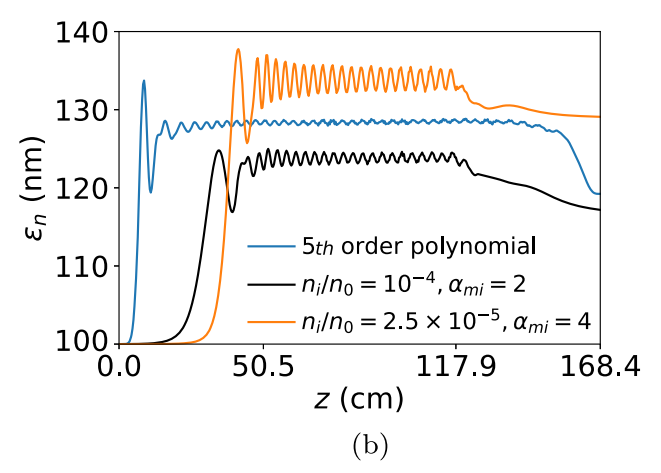


FIG. 5. (a) Symmetric plasma density profiles used for a 100 GeV witness beam. The upramp in blue is the same as in Fig. 4. The density profile in black is the same as in Fig. 2(a). The α_{mi} is now 2 rather than 1 because the initial energy is 4 times higher (100 GeV compared to 25 GeV). The orange profile has a lower density at the entrance such that the initial σ_m is the same as in Fig. 2, but with a higher adiabaticity ($\alpha_{mi} = 4$). (b) Projected emittance evolution for a 100 GeV witness beam when matching to the corresponding ramps in (a).

at the plasma entrance. It is worth noting that for an adiabatic ramp (where the density does not vanish at the entrance), the CS parameters calculated using this numerical backward propagation agree with the matched CS parameters defined in Eq. (2). We then initialize the witness beam's CS parameters using β_i , α_i in QPAD. The solid green and orange curves in Fig. 4 show the actual evolution of the CS parameters. Initially, they follow the backward-propagated β and α because the density is low near the entrance such that the matched beam spot size is large. Therefore, ion motion effects are small and Eq. (5) is valid. Ion motion starts to play a role when the solid curves and the dashed curves deviate from each other where the beam has already entered the adiabatic region. The solid red curve in Fig. 4 shows the emittance evolution from a QPAD simulation for the entire plasma density profile shown (upramp, plateau, and downramp) in the blue curve in Fig. 5(a). As before, the emittance evolution reverses in the downramp, and the overall emittance growth is around only 13%.

We note that for a given length of the ramp, there is a trade-off between minimizing the initial ion motion and maintaining the adiabaticity of the plasma ramp. This can be seen by substituting z = 0 in Eq. (3),

$$\frac{n_i}{n_0} = \left(1 + \frac{\alpha_{mi}L}{\beta_{m0}}\right)^{-2},\tag{6}$$

where n_i increases as α_{mi} decreases and vice versa. Thus in order to have less initial ion motion by decreasing n_i , we need to sacrifice the adiabaticity of the plasma ramp, and vice versa.

A TeV-class PBA-LC may require limiting emittance growth more than 20+ stages during which the witness beam energy will be higher for the later stages. As can be seen from Eq. (1), the matched spot size scales as $\gamma^{-1/4}$. Therefore, ion motion and emittance growth will be more severe in the later stages. To examine this scaling, we carried out simulations with a 100 GeV witness beam. We used the three different plasma density ramps shown in Fig. 5(a). The blue upramp is for the same profile used in Fig. 4. We match the witness beam through the numerical backward propagation of Eq. (5). The black profile is the same as the solid black curve in Fig. 2, with the expression of the upramp given by Eq. (3). However, in this case $\alpha_{mi} \sim 2$ since the witness beam's energy is 100 GeV. Furthermore, since the beam's energy is higher, σ_{mi} is smaller leading to more initial ion motion. The orange upramp is also described by Eq. (3) but with $n_i/n_0 = 2.5 \times 10^{-5}$, ensuring the same initial matched spot size, σ_{mi} , as the 25 GeV case. However, from Eq. (6), the use of a lower density leads to a larger $\alpha_{mi} \sim 4$, such that the adiabatic condition is severely violated. For the black and orange profiles, we match the witness beam directly to the entrance rather than back propagate Eq. (5). Figure 5(b) shows the projected emittance evolution corresponding to the profiles in Fig. 5(a). We can see that the emittance growth of a 100 GeV witness beam can be limited to less than 20% if we appropriately choose the plasma density ramp and match the beam.

This work was supported by the U.S. Department of Energy (DOE) High Energy Physics (HEP) under Grant No. DE-SC0010064 and SciDAC through an FNAL subcontract No. 644405 and an LBNL subcontract No. 7350365:1, the National Science Foundation Grant No. 2108970, and the National Natural Science Foundation of China (NSFC) Grant No. 12075030. The simulations were carried out on Cori at NERSC.

^[1] C. Joshi, S. Corde, and W. B. Mori, Phys. Plasmas **27**, 070602 (2020).

^[2] J. B. Rosenzweig, B. Breizman, T. Katsouleas, and J. J. Su, Phys. Rev. A 44, R6189 (1991).

- [3] W. Lu, C. Huang, M. Zhou, W. B. Mori, and T. Katsouleas, Phys. Rev. Lett. 96, 165002 (2006).
- [4] T. Mehrling, J. Grebenyuk, F. S. Tsung, K. Floettmann, and J. Osterhoff, Phys. Rev. ST Accel. Beams 15, 111303 (2012).
- [5] C. Joshi, E. Adli, W. An, C. E. Clayton, S. Corde, S. Gessner, M. J. Hogan, M. Litos, W. Lu, K. A. Marsh, W. B. Mori, N. Vafaei-Najafabadi, B. O'shea, X. Xu, G. White, and V. Yakimenko, Plasma Phys. Controlled Fusion 60, 034001 (2018).
- [6] K. Floettmann, Phys. Rev. ST Accel. Beams 17, 054402 (2014).
- [7] I. Dornmair, K. Floettmann, and A. R. Maier, Phys. Rev. ST Accel. Beams 18, 041302 (2015).
- [8] X. L. Xu, J. F. Hua, Y. P. Wu, C. J. Zhang, F. Li, Y. Wan, C.-H. Pai, W. Lu, W. An, P. Yu, M. J. Hogan, C. Joshi, and W. B. Mori, Phys. Rev. Lett. 116, 124801 (2016).
- [9] R. Ariniello, C. Doss, K. Hunt-Stone, J. Cary, and M. Litos, Phys. Rev. Accel. Beams 22 (2019).
- [10] M. D. Litos, R. Ariniello, C. E. Doss, K. Hunt-Stone, and J. R. Cary, Phil. Trans. R. Soc. A 377, 20180181 (2019).
- [11] X. Li, A. Chancé, and P. A. P. Nghiem, Phys. Rev. Accel. Beams 22, 021304 (2019).
- [12] Y. Zhao, W. An, X. Xu, F. Li, L. Hildebrand, M. Hogan, V. Yakimenko, C. Joshi, and W. Mori, Phys. Rev. Accel. Beams 23, 011302 (2020).
- [13] A. Seryi, M. Hogan, S. Pei, T. Raubenheimer, P. Tenenbaum, T. Katsouleas, C. Huang, C. Joshi, W. Mori, and P. Muggli, in *Proceedings of the 23rd Particle*

- Accelerator Conference, Vancouver, Canada, 2009 (IEEE, Piscataway, NJ, 2009), WE6PFP081.
- [14] S. Lee and T. Katsouleas, AIP Conf. Proc. **472**, 524 (1999).
- [15] J. B. Rosenzweig, A. M. Cook, A. Scott, M. C. Thompson, and R. B. Yoder, Phys. Rev. Lett. 95, 195002 (2005).
- [16] W. An, W. Lu, C. Huang, X. Xu, M. J. Hogan, C. Joshi, and W. B. Mori, Phys. Rev. Lett. 118, 244801 (2017).
- [17] R. Gholizadeh, T. C. Katsouleas, P. Muggli, C. K. Huang, and W. B. Mori, Phys. Rev. Lett. 104, 155001 (2010).
- [18] C. Benedetti, C. B. Schroeder, E. Esarey, and W. P. Leemans, Phys. Rev. Accel. Beams 20, 111301 (2017).
- [19] C. Benedetti, T. J. Mehrling, C. B. Schroeder, C. G. R. Geddes, and E. Esarey, Phys. Plasmas 28, 053102 (2021).
- [20] R. L. Williams and T. Katsouleas, AIP Conf. Proc. 279, 565 (1992).
- [21] F. Li, W. An, V. K. Decyk, X. Xu, M. J. Hogan, and W. B. Mori, Comput. Phys. Commun. 261, 107784 (2021).
- [22] C. Huang, V. Decyk, C. Ren, M. Zhou, W. Lu, W. Mori, J. Cooley, T. Antonsen, and T. Katsouleas, J. Comput. Phys. 217, 658 (2006).
- [23] W. An, V. K. Decyk, W. B. Mori, and T. M. Antonsen, J. Comput. Phys. 250, 165 (2013).
- [24] M. Tzoufras, W. Lu, F. S. Tsung, C. Huang, W. B. Mori, T. Katsouleas, J. Vieira, R. A. Fonseca, and L. O. Silva, Phys. Rev. Lett. 101, 145002 (2008).
- [25] T. N. Dalichaouch, X. L. Xu, A. Tableman, F. Li, F. S. Tsung, and W. B. Mori, Phys. Plasmas 28, 063103 (2021).
- [26] P. G. O'Shea, Phys. Rev. E 57, 1081 (1998).
- [27] S. Y. Lee, *Accelerator Physics* (World Scientific Publishing Co. Pte. Ltd., Singapore, 2004), 2nd ed.